Regular Article

blood

THROMBOSIS AND HEMOSTASIS

Complex formation with pentraxin-2 regulates factor X plasma levels and macrophage interactions

Vincent Muczynski,[1,2] Gabriel Aymé,[1] Véronique Regnault,[3] Marc Vasse,[1,4] Delphine Borgel,[1,5] Paulette Legendre,[1] Amine Bazaa,[1] Amélie Harel,[1] Cécile Loubière,[1] Peter J. Lenting,[1] Cécile V. Denis,[1,*] and Olivier D. Christophe[1,*]

[1]Institut National de la Santé et de la Recherche Médicale, Unité Mixte de Recherche (UMR)_S 1176, University Paris-Sud, Université Paris-Saclay, Le Kremlin-Bicêtre, France; [2]Inovarion SAS, Paris, France; [3]Institut National de la Santé et de la Recherche Médicale, UMR_S 1116, Université de Lorraine, Vandoeuvre-lès-Nancy, France; [4]Biology Department, Hôpital Foch, Suresnes, France; and [5]Assistance Public–Hôpiteaux de Paris, Service d'Hématologie Biologique, Hôpital Necker, Paris, France

Key Points

- We have identified PTX2 as a novel partner for FX in the circulation, and their plasma levels are interdependent.
- FX and PTX2 cooperate with SR-AI to prevent their uptake by macrophages.

Recently, we have identified scavenger receptor class A member I (SR-AI) as a receptor for coagulation factor X (FX), mediating the formation of an FX reservoir at the macrophage surface. Here, we demonstrate that the FX/SR-AI-complex comprises a third protein, pentraxin-2 (PTX2). The presence of PTX2 is essential to prevent internalization of FX by SR-AI, and the presence of FX is needed to interfere with internalization of PTX2. Binding studies showed that FX, SR-AI, and PTX2 independently bind to each other ($K_{D,app}$: 0.2-0.7 μM). Surprisingly, immunoprecipitation experiments revealed that FX and PTX2 circulate as a complex in plasma, and complex formation involves the FX activation peptide. No binding of PTX2 to other vitamin K–dependent proteins was observed. Short hairpin RNA–mediated inhibition of PTX2 levels in mice resulted not only in reduced levels of PTX2, but also in similarly reduced FX levels. Moreover, PTX2 and FX levels were correspondingly reduced in SR-AI–deficient mice. Analysis of 71 human plasma samples uncovered a strong correlation between FX and PTX2 plasma levels. Furthermore, plasma samples of patients with reduced FX levels (congenital/acquired FX deficiency or after anti–vitamin K treatment) were characterized by concomitantly decreased PTX2 levels. In conclusion, we identified PTX2 as a novel partner for FX, and both proteins cooperate to prevent their SR-AI–mediated uptake by macrophages. Interestingly, their respective plasma levels are interdependent. These findings seem of relevance in perspective of ongoing clinical trials, in which plasma depletion of PTX2 is used as a therapeutical approach in the management of systemic amyloidosis. (*Blood.* 2017;129(17):2443-2454)

Introduction

Vitamin K–dependent factor X (FX) is best known for its central role in hemostasis. Its functional deficiency is associated with severe bleeding, including epistaxis, hemarthrosis, and gastrointestinal bleeding.[1,2] However, FX also functions beyond hemostasis, as was first recognized from the partial embryonic lethality of FX-deficient mice that was seemingly unrelated to bleeding complications.[3] Other examples of nonhemostatic functions for FX include inhibition of angiogenesis,[4] regulation of the immune response toward viral infections,[5-9] and stimulation of proinflammatory and profibrotic responses in fibroblasts.[10-12] The multiplicity of biological functions of FX emphasize the importance of understanding how physiological levels of FX are regulated. In search of these mechanisms, we recently discovered that this regulation was quite unusual compared with other proteins and strongly depends on interactions between FX and macrophages.[13,14]

The pertinent role of macrophages first became apparent when it was found that chemical depletion of macrophages reduces FX levels by 60% to 70%.[13] Biodistribution and cell-based experiments then revealed that FX accumulates at the surface of several types of macrophages, including liver Kupffer cells.[13] After prolonged incubation at 37°C, no degradation of FX was detected, and no colocalization with endosomal markers was observed.[13,14] Instead, FX was released from the macrophage surface as an intact functional protein.[13] Apparently, the macrophage surface represents a reservoir for FX proteins. This was surprising, knowing that macrophages are efficient in scavenging other hemostatic proteins, such as the FVIII/von Willebrand factor (VWF) complex.[15]

We have recently undertaken studies to decipher the molecular basis of the FX-macrophage interaction. By doing so, we were able to identify scavenger receptor class A member I (SR-AI) as the main (if not only) receptor for FX at the macrophage surface.[14] FX colocalizes with SR-AI at the cell surface, whereas no binding of FX to SR-AI–deficient macrophages could be detected. In addition, FX displays dose-dependent binding to the recombinant ectodomain of SR-AI. Importantly, SR-AI–deficient mice have strongly reduced levels of FX (30% to 40% of normal), and the antibody-mediated inhibition of SR-AI results in increased clearance of the FX protein in mice.[14] Apparently, SR-AI plays a central role in the protective effect that macrophages have regarding the regulation of FX plasma levels.

What remained unresolved in our previous study is the notion that although SR-AI is known for its high endocytic capacity of acetylated low-density lipoprotein,[14,16,17] it binds but does not internalize FX. Here,

Submitted 24 June 2016; accepted 11 February 2017. Prepublished online as *Blood* First Edition paper, 17 February 2017; DOI 10.1182/blood-2016-06-724351.

The publication costs of this article were defrayed in part by page charge payment. Therefore, and solely to indicate this fact, this article is hereby marked "advertisement" in accordance with 18 USC section 1734.

*C.V.D. and O.D.C. contributed equally to this study.

The online version of this article contains a data supplement.

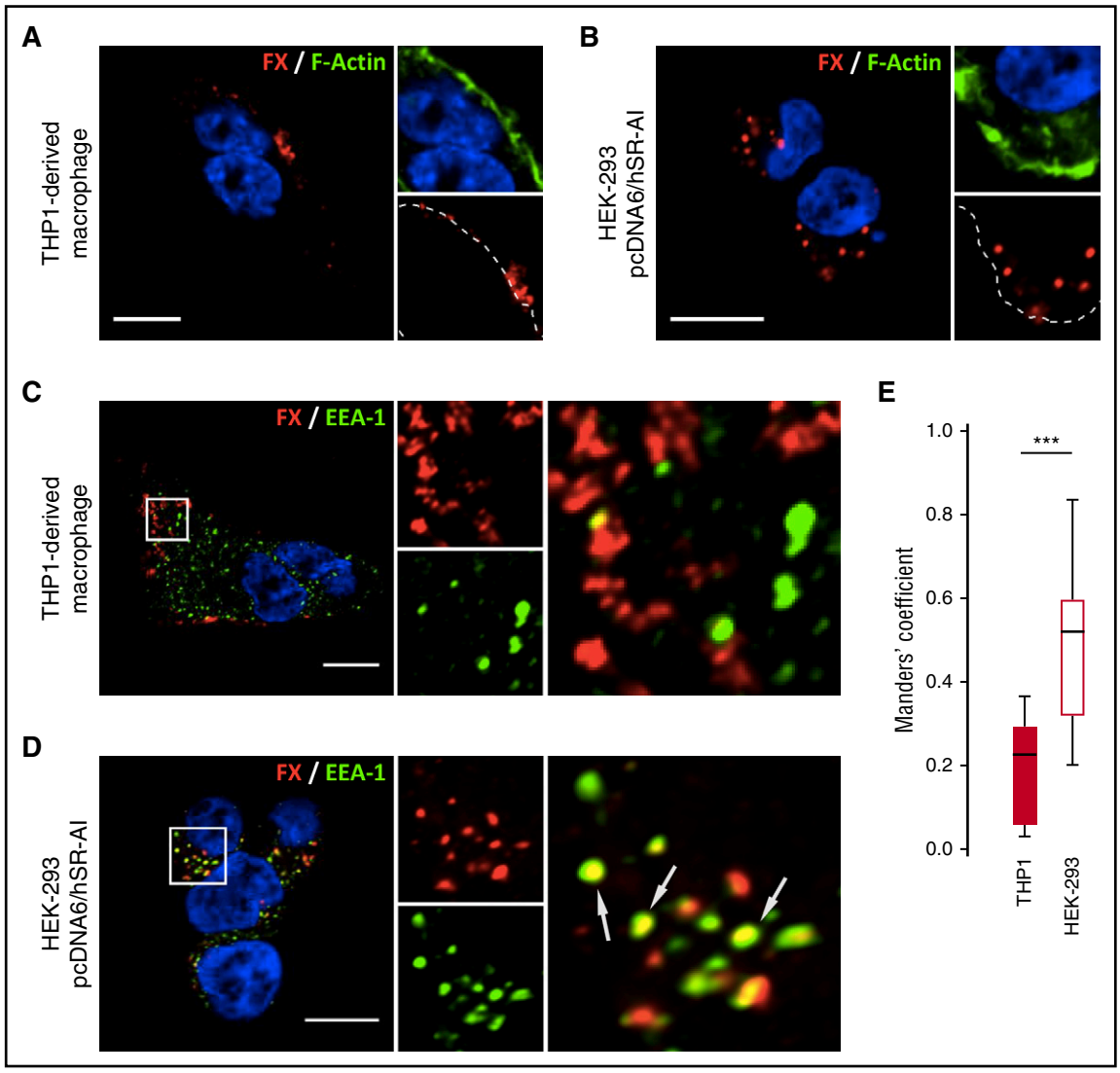

Figure 1. FX is internalized by SR-AI in HEK293 cells but not in THP1-derived macrophages. THP1-derived macrophages (A,C) or SR-AI–expressing HEK-293 (B,D) were incubated with FX for 1 hour at 37°C. FX was immunostained (red) along with polymerized actin counterstaining using Alexa488-labeled phalloïdin (A-B) or EEA-1 immunostaining (C-D). Dotted lines define cell boundaries based on phalloïdin staining (A-B), and arrows indicate spots of colocalization (C-D). Images were acquired in confocal microscopy (objective 63×, *z*-depth 1 μm). Bars represent 10 μm. (E) FX colocalization with EEA-1 was quantified by calculating the tMC for FX using JACoP plugin in Fiji software. The results are expressed in a whisker plot where boxes represent the median and 25th to 75th percentile and bars represent the minimum and maximum of 10 to 11 cells in 3 different experiments. ***$P < .001$ in a Mann-Whitney nonparametric unpaired statistical test.

we investigated the mechanism allowing FX to remain at the macrophage surface while being bound to SR-AI, hypothesizing that another partner is needed to prevent internalization of the FX/SR-AI complex. Mass spectrometry and coimmunoprecipitation approaches were employed to identify potential candidates. We identified pentraxin-2 (PTX2) as a so far unidentified FX-binding protein. PTX2 forms a complex with FX in plasma and prevents internalization of the FX/SR-AI complex. Moreover, FX and PTX2 levels appear to be interdependent. As such, PTX2 contributes to the mechanism that maintains normal FX plasma levels and allows the accumulation of FX at the macrophage surface.

Material and methods

An extensive description of the experimental procedure can be found in the supplemental Methods (available on the *Blood* Web site), a brief summary of which is given subsequently.

Ethics statement

Human subjects. Blood and residual plasma were obtained from healthy volunteers and patients, respectively. The study was approved by local ethics committees of University Hospital Bicêtre (Centre Hospitalier Universitaire [CHU]-Bicêtre), CHU-Nancy, CHU-Necker, and Hospital Foch and conducted according to the Declaration of Helsinki. For animal experiments, housing and experiments were done as recommended by French regulations and the experimental guidelines of the European Community. This project was approved by the local ethical committee CEEA 26 (# 2012-036).

Cell-culture and binding experiments

THP1-derived and monocyte-derived macrophages and SR-AI–expressing HEK293 cells were used in the study. Cell-binding experiments were analyzed with immunofluorescent staining using widefield and confocal microscopy. All images were analyzed and assembled using ImageJ software.

Mass spectrometry

Exogenous FX was incubated in a total protein extract prepared from THP1-derived macrophages and subsequently immunoprecipitated.

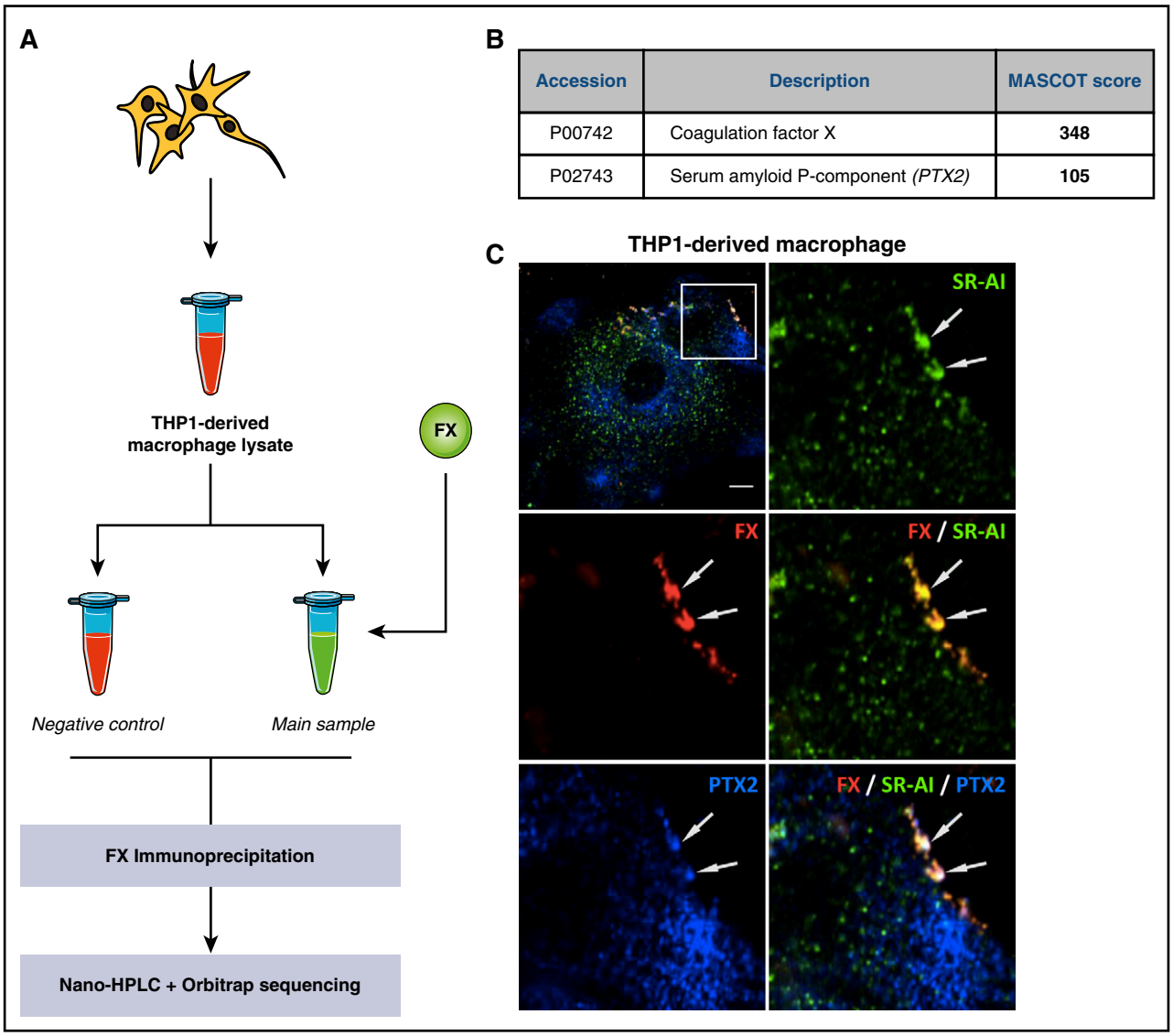

Accession	Description	MASCOT score
P00742	Coagulation factor X	**348**
P02743	Serum amyloid P-component *(PTX2)*	**105**

Figure 2. Identification of PTX2 as a potential partner for FX. THP1-derived macrophage lysate was incubated with (main sample) or without (control) FX for 1 hour. FX was immunoprecipitated, and the collected material was analyzed for identification of potential FX partners using nano-HPLC separation and Orbitrap sequencing of the different peptides (A). Data were processed through the MASCOT algorithm to identify peptides and corresponding proteins. Positive candidates were proteins not detected in the control sample and detected in the FX-incubated sample with a MASCOT detection score >100 in 2 different experiments (B). (C) THP1-derived macrophages were immunostained for FX (red), PTX2 (blue), and SR-AI (green), and representative images were acquired in confocal microscopy. Arrows indicate area of triple colocalization. Bar represents 10 μm; objective 63×, *z*-depth 1 μm.

Coimmunoprecipitated material was analyzed by nano–high-pressure liquid chromatography (nano-HPLC) separation and Orbitrap-sequencing. Peptide sequences were identified and analyzed using MASCOT software (Matrix Science, Boston, MA).

Biolayer interferometry (BLI)

Binding was assessed via BLI analysis using Octet-QK equipment (Fortebio, Meldo Park, CA) with purified proteins. Apparent K_D ($K_{D,app}$) was calculated employing the Michaelis-Menten equation.

Coimmunoprecipitation and western blot analysis

FX and PTX2 were coimmunoprecipitated from normal human plasma, FX-immunodepleted plasma, or FX-immunodepleted plasma supplemented with FX, FX_N181A, or FXa. Analyses were performed by sodium dodecyl sulfate–polyacrylamide gel electrophoresis followed by anti-PTX2 or anti-FX immunoblotting.

Mice

For short hairpin (shRNA) experiments, specific shRNA anti-murine PTX2 (Origene, Rockville, MD) was expressed in C57Bl/6 wild-type (wt) mice using the hydrodynamic gene transfer.[18] Controls were performed by the injection of nonrelevant scramble shRNA. For clearance experiments, C57Bl/6 or SR-AI–deficient mice were given FX or the FX_N181A variant intravenously, and residual FX was measured over time. The recovery was calculated as the percentage of residual FX at time point 5 minutes.

Results

FX is internalized by SR-AI–transfected HEK293 cells but not by macrophages

To explore the endocytic ability of SR-AI toward FX, we compared the binding of FX to THP1-derived macrophages and SR-AI–transfected

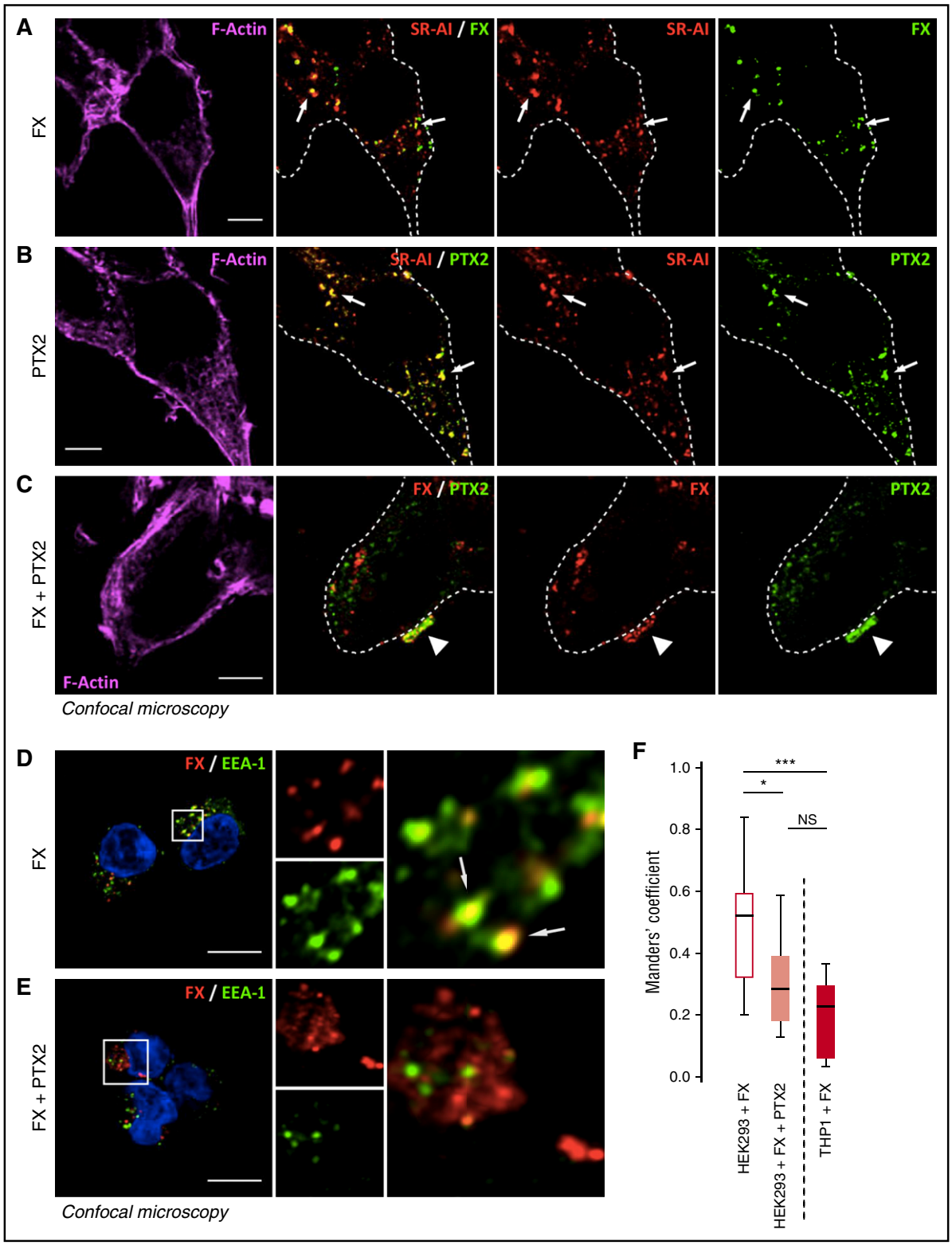

Figure 3. PTX2 reduces FX internalization in SR-AI–expressing HEK293 cells. SR-AI–expressing HEK293 cells were incubated with 150 nM of FX (A), 500 nM of PTX2 (B), or both (C) for 1 hour at 37°C and then washed and fixed. Representative confocal microscopy images of FX or PTX2 immunostaining along with SR-AI (A-B) or coimmunostaining of FX and PTX2 (C) are depicted. FX (red) and EEA-1 (green) were immunostained in SR-AI–expressing HEK293 cells incubated with either FX (D) or FX + PTX2 (E), and images were acquired in confocal microscopy. FX colocalization with EEA-1 was quantified by calculating the tMC for FX using JACoP plugin in Fiji software (F). Results are expressed in a whisker plot where boxes represent the median and 25th to 75th percentile, and bars represent the minimum and maximum of 10 to 11 cells in 3 different experiments. *$P < .05$; ***$P < .001$ in a Mann-Whitney nonparametric unpaired statistical test. N.S., not significant. In representative confocal images, dotted lines define cell boundaries based on phalloïdin staining, arrows indicate internalized FX or PTX2 colocalized with SR-AI (A-B) or area of colocalization between FX and SR-AI (D), and arrowheads indicate colocalization between FX and PTX2 (C). Objective 63×, *z*-depth 1 μm; bars represent 10 μm.

HEK293 cells. Following incubation (1 hour at 37°C), confocal microscopy analyses revealed clusters of accumulated FX localized at the surface of THP1-derived macrophages (Figure 1A). In contrast, FX was detected inside the cells when incubated with SR-AI–expressing HEK293 cells, indicating potential endocytosis (Figure 1B). Upon simultaneous staining for FX and early endosome antigen-1 (EEA-1), no visual colocalization within THP1-derived macrophages was detected, whereas visible areas of colocalization for FX and EEA-1 were observed within SR-AI–expressing HEK293 cells (Figures 1C-D). In order to quantify colocalization between FX and EEA-1, cell stacks acquired in confocal microscopy were analyzed to calculate the thresholded Mander's coefficient (tMC). THP1-derived macrophages incubated with FX had a tMC of 0.20 ± 0.12 (mean ± standard deviation [SD]), whereas SR-AI–expressing HEK293 cells had a tMC value of 0.50 ± 0.17 ($P < .001$; Figure 1E). This statistical difference in tMC value confirms that the FX signal truly overlaps the EEA-1 signal in HEK293 cells but not in THP1-derived macrophages. Thus, SR-AI has the intrinsic capacity to bind and internalize FX but is unable to do so when expressed in macrophages. This points to the presence of an element that interferes with the internalization of the FX/SR-AI complex in these cells.

Mass spectrometry identifies PTX2 as a partner of FX in macrophages

In search of the element preventing internalization of the FX/SR-AI complex in macrophages, FX was incubated with a protein extract of THP1-derived macrophage and subsequently immunoprecipitated using magnetic beads coated with anti-FX antibodies. Control samples were prepared without adding FX. Both precipitates were analyzed via nano-HPLC/Orbitrab mass spectrometry for peptide sequences (Figure 2A). Two proteins with an arbitrary MASCOT score >100 were only detected in the FX-incubated sample. As expected, the most abundant protein was FX. The second protein was PTX2, also known as serum amyloid P-component (accession number P02743). Identifying PTX2 as a macrophage-produced protein was surprising, because hepatocytes are reportedly the main source of PTX2.[19,20] However, additional confocal microscopy analysis of THP1-derived macrophages confirmed that areas enriched in FX and SR-AI also contain PTX2 (Figure 2C). The presence of a ternary complex was further verified using Duolink–Proximity Ligation Assay analysis, using antibody combinations against each possible pair: FX/SR-AI, FX/PTX2, and PTX2/SR-AI. In THP1-derived and primary $CD14^+$ cell–derived macrophages, a positive signal for each combination was detected (supplemental Figure 1). Interestingly, a positive signal was also observed for PTX2/SR-AI without FX, indicating that macrophage-produced PTX2 spontaneously associates with SR-AI. Because expression of SR-AI and/or PTX2 may depend on the macrophage phenotype, we also analyzed binding of FX to macrophages of the M0, M1, and M2 phenotypes. Relative to M0 macrophages, the presence of PTX2/SR-AI complexes were increased 1.4-fold and reduced 2-fold on M1 and M2 macrophages, respectively (supplemental Figure 2). However, we could not detect significant differences in FX binding to each of these macrophages (supplemental Figure 2). Together, these data identify PTX2 as a potential candidate involved in the regulation of FX/SR-AI internalization.

PTX2 modulates SR-AI–mediated internalization of FX

To determine if PTX2 modulates endocytosis of the FX/SR-AI complex, we incubated FX and/or PTX2 with SR-AI–transfected HEK293 cells for 1 hour at 37°C. Subsequently, confocal microscopy was used to determine the residual staining of FX, PTX2, or the complex (Figure 3A-C). When added individually, both FX and PTX2 were associated with SR-AI within the cellular borders, indicating that both proteins were endocytosed via SR-AI. Some residual uptake of FX and PTX2 was also observed when applied together (Figure 3C). However, patches of FX/PTX2 staining were found at the cell surface, indicating that these proteins resisted internalization (Figure 3C). Moreover, this complex remained at the cell surface even when analyzed after incubating 2 more hours at 37°C, whereas FX alone was no longer detectable under these conditions (supplemental Figure 3). The notion that FX internalization by SR-AI was strongly reduced in the presence of PTX2 was confirmed in control experiments assessing colocalization of FX with the early endosomal marker EEA-1. Whereas FX alone colocalized with EEA-1, little, if any, colocalization was observed when FX was incubated in the presence of PTX2 (Figure 3D-F). Thus, PTX2 and FX participate in complex formation with SR-AI at the cell surface, and formation of this ternary complex prevents internalization of both FX and PTX2.

Molecular interaction between FX, SR-AI, and PTX2: BLI analysis, immunoprecipitation, and FX activation

Molecular interactions between FX, SR-AI, and PTX2 were then assessed through BLI experiments using purified proteins. All 3 proteins did interact independently with each other in a dose-dependent manner (Figure 4A-C). Apparent dissociation constants ($K_{D,app}$) were calculated from the association curves for the different protein combinations using the Michaelis-Menten equation. The respective $K_{D,app}$ values were calculated to be 0.21 ± 0.04 μM, 0.65 ± 0.10 μM, and 0.73 ± 0.15 μM for the interactions between SR-AI and PTX2, SR-AI and FX, and FX and PTX2, respectively (Figure 4A-D). In separate binding experiments, we noted that FX had similar binding efficiency to SR-AI alone or to the PTX2/SRA1 complex (supplemental Figure 4). Binding to PTX2 seemed specific for FX, as no significant association of FVII, FIX, or protein C could be detected (supplemental Figure 4).

Interestingly, the $K_{D,app}$ value for the interaction between FX and PTX2 is close to their plasma concentrations (0.17 μM and 1.2 μM for FX and protomer PTX2, respectively), suggesting that both proteins may form spontaneous complexes in the circulation. This possibility was tested in complementary immunoprecipitation studies using normal and FX-depleted human plasma. PTX2 was coprecipitated with FX, while FX could be coprecipitated with PTX2 (Figure 4E, lanes 1 and 3). No complex could be precipitated from FX-deficient plasma (Figure 4E, lanes 2 and 4), unless it was replenished with purified FX (Figure 4E, lane 5). In contrast, we could further not detect any immunoprecipitation if FX-deficient plasma was replenished with FXa or FX with the N181A mutation, which deletes an N-glycan in the activation peptide (Figure 4F). We finally addressed the effect of PTX2 on FX activation and did not observe any differences in the kinetics of FX activation by the FVIIa/TF or tenase complex or RVV-X protease (Figure 4G). Altogether, these data demonstrate that FX, SR-AI, and PTX2 may interact with each other, and that FX and PTX2 may already form a complex in plasma.

Role of SR-AI in the regulation of the PTX2/FX circulating complex

Having identified that FX and PTX2 circulate in the plasma as a macromolecular complex, we investigated to what extent plasma levels of FX and PTX2 are interrelated. Hydrodynamic plasmid delivery was used to induce expression of shRNA targeting murine PTX2 in wt C57Bl/6 mice to interfere with the hepatic expression of PTX2.

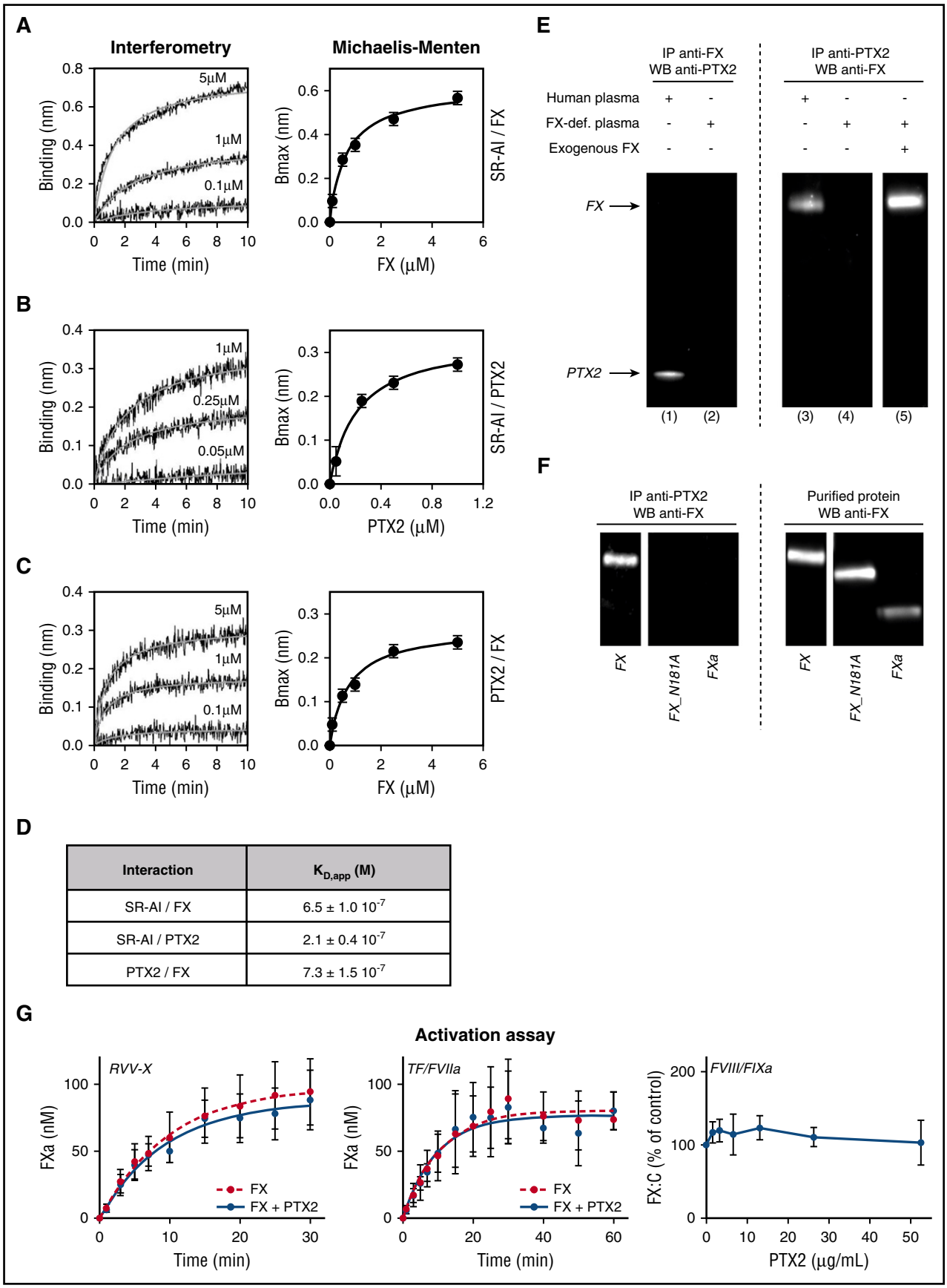

Interaction	$K_{D,app}$ (M)
SR-AI / FX	$6.5 \pm 1.0\ 10^{-7}$
SR-AI / PTX2	$2.1 \pm 0.4\ 10^{-7}$
PTX2 / FX	$7.3 \pm 1.5\ 10^{-7}$

Figure 4. Molecular interactions between FX, SR-AI, and PTX2. Representative BLI graphs (Octet) of molecular binding between FX, SR-AI, and PTX2. Ten micrograms per milliliter of recombinant SR-AI (A-B) or purified PTX2 (C) were coated on the biosensor, and association with increasing concentrations (0.1 to 5 μM) of FX (A,C) or increasing concentrations (0.05 to 1 μM) of purified PTX2 (B) were measured over an association phase of 600 seconds. Results are expressed as the wavelength shift

Residual levels of PTX2, FX, and FIX were measured 24 hours after injection. Circulating PTX2 antigen levels were reduced to 56 ± 21% (mean ± SD; $P < .01$) in PTX2 shRNA-treated mice compared with control shRNA-treated mice (Figure 5A). Residual FIX activity levels remained unchanged in both control and PTX2 shRNA-treated mice ($P > .05$; Figure 5A). In contrast, the expression of PTX2 shRNA induced a significant reduction in levels of endogenous FX activity (63 ± 26% compared with control mice; n = 10; $P < .01$; Figure 5A). Importantly, the application of PTX2 shRNA left the number of macrophages unaffected (Figure 5B-C). Furthermore, VWF antigen levels were unaffected after shRNA treatment, indicating that the endocytic function of macrophages was conserved (Figure 5A). Together, these findings point to a concomitant reduction in circulating levels of both FX and PTX2.

Given these results in combination with the notions that FX and PTX2 form a complex in plasma (Figure 4E-F) and that SR-AI–deficient mice have strongly reduced FX levels (Figure 5D),[14] we analyzed plasma samples from SR-AI–deficient and control wt mice for the presence of PTX2 antigen. PTX2 levels were significantly reduced to 45.5 ± 14.6% (mean ± SD; n = 7; $P < .001$; Figure 5D), confirming a link between SR-AI and plasma levels of FX and PTX2. The relationship was further illustrated when analyzing the correlation between plasma levels of FX and PTX2 in both wt and SR-AI–deficient mice: a statistically significant correlation could be calculated (Spearman r correlation 0.93; $P < .0001$; Figure 5E) in this regard.

Clearance of FX and FX_N181A in wt and SR-AI–deficient mice

To further analyze how the formation of the SR-AI/PTX2/FX complex affects clearance of FX, a series of clearance experiments were performed. First, clearance of wt-FX in wt and SR-AI mice was performed. In agreement with previous data using SR-AI blocking antibodies,[14] FX was cleared more rapidly in SR-AI–deficient mice compared with wt mice (Figure 5F). As for mutant FX_N181A (which is unable to interact with PTX2), clearance was increased to a similar extent as wt FX in SR-AI–deficient mice (Figure 5G). Interestingly, the increased clearance of this mutant was independent of the mouse strain that was used (wt or SR-AI–deficient mice), demonstrating that the absence of SR-AI does not delay or enhance FX clearance when FX is not in complex with PTX2. Thus, the ability of FX to interact with both SR-AI and PTX2 is needed avoid accelerated clearance of FX by a so far unidentified clearance mechanism.

FX and PTX2 levels are correlated in human plasma

In view of the data obtained in mice, we next analyzed plasma levels of FX and PTX2 in a series of 71 plasma samples from healthy individuals. As depicted in Figure 6A, a statistically relevant correlation was observed between levels of FX and PTX2 (Spearman r correlation 0.40; $P = .0006$). In addition, we analyzed plasmas of patients diagnosed with an FX deficiency (either acquired or congenital) and patients receiving anti–vitamin K treatment. In both cases, the reduction in FX plasma levels was associated with a concomitant reduction in plasma levels of PTX2 (Figure 6B). This further provides support for our findings that plasma levels of FX and PTX2 are interdependent. In conclusion, our study identifies PTX2 as a novel partner for FX in plasma and for the FX/SR-AI complex. The formation of the SR-AI/PTX2/FX complex is necessary to maintain normal plasma levels of FX and PTX2 (Figure 7).

Discussion

The main function of macrophage scavenger receptors is to remove soluble elements from the circulation by targeting them to intracellular degradation pathways. It was surprising therefore, that the association of coagulation FX to the macrophage-receptor SR-AI resulted in an accumulation of FX at the cell surface rather than in its internalization and degradation.[13,14] Indeed, no activation of FX at the surface of THP1-derived macrophages could be detected, even after 1 hour incubation at 37°C (supplemental Figure 5). Hence, the objective of the present study was to address the question as to why FX remains at the cellular surface while in complex with the endocytic receptor SR-AI. Unexpectedly, we identified PTX2 as a protein that associates to both FX and SR-AI, and the presence of PTX2 allows the formation of a ternary complex (FX/PTX2/SR-AI) at the macrophage surface that prevents internalization of FX and PTX2 (Figures 2-4). In addition, we provide evidence that FX and PTX2 circulate as a complex in plasma, and that their respective plasma levels are interdependent (Figures 4-6).

The identification of PTX2 as a potential macrophage-derived partner for FX was unforeseen, given that hepatocytes are reportedly the main source of PTX2.[19,20] Nonetheless, the presence of human PTX2 at the surface of macrophages was confirmed via confocal immunofluorescence microscopy and Duolink–Proximity Ligation Assay analysis (Figure 2; supplemental Figures 1 and 2). We considered the option that PTX2 in the macrophages originated from the cell-culture medium. However, the peptide sequences of PTX2 corresponded to human PTX2 rather than bovine PTX2. In addition, PTX2 was also absent in the FX preparations used throughout the study (not shown), indicating that the cells have not been exposed to an outside source of human PTX2. The identification of PTX2 in human macrophages suggests that cells other than hepatocytes may be capable of producing the PTX2 protein.

FX binding to the SR-AI/PTX2 complex was independent of the origin of the macrophage (THP1- or monocyte-derived macrophages) or its activation state (M0 vs M1 or M2 macrophages; supplemental Figure 2). Because a near complete overlap between FX and CD68 staining in liver tissue sections was previously reported,[13] we assume that both bone marrow–derived macrophages and those not derived from bone marrow (both of which constitute the Kupffer cell population)[21] are able to bind FX independently of their activation state. Furthermore, binding to macrophages is probably not limited to the liver, as biodistribution experiments detected FX also in other organs, such as spleen and kidney.[13]

Figure 4 (continued) (in nm) generated by the binding of the different molecules. Apparent K_D values were calculated using the Michaelis-Menten equation (D). (E) Coimmunoprecipations of FX and PTX2 were performed in normal human plasma (lanes 1 and 3) and FX-deficient plasma (lanes 2, 4, and 5) supplemented or not with 10 μg/mL of FX (lane 5). Immunoprecipitates were analyzed by western blot using anti-FX and anti-PTX2 antibodies. (F) Coimmunoprecipitations of PTX2 were performed in FX-deficient plasma supplemented with 10 μg/mL of FX, FX_N181A mutant, or activated FXa. Immunoprecipitates or purified proteins (10 ng per lane) were analyzed with an anti-FX antibody by western blot. (G) FX (100 nM) preassociated (blue circles) or not (red circles) with 1 μM of PTX2 was incubated with Russel's Viper Venom X (RVV-X) enzyme (left panel) or tissue factor/FVIIa (TF/FVIIa) and phospholipids (middle panel). Kinetic conversion of FX into FXa was monitored during a 30-minute (RVV-X) or 60-minute (TF/FVIIa) time course. Right panel represents effect of different PTX2 concentrations (0-52.5 μg/mL) on FX activation by the FIXa/FVIIIa complex in the presence of phospholipid vesicles. Concentrations were 42 nM FX, 20 pM FIXa, and 5 pM thrombin-activated FVIII, and FXa generation was allowed for 5 minutes. Graphs represent the mean ± SD of 3 different experiments.

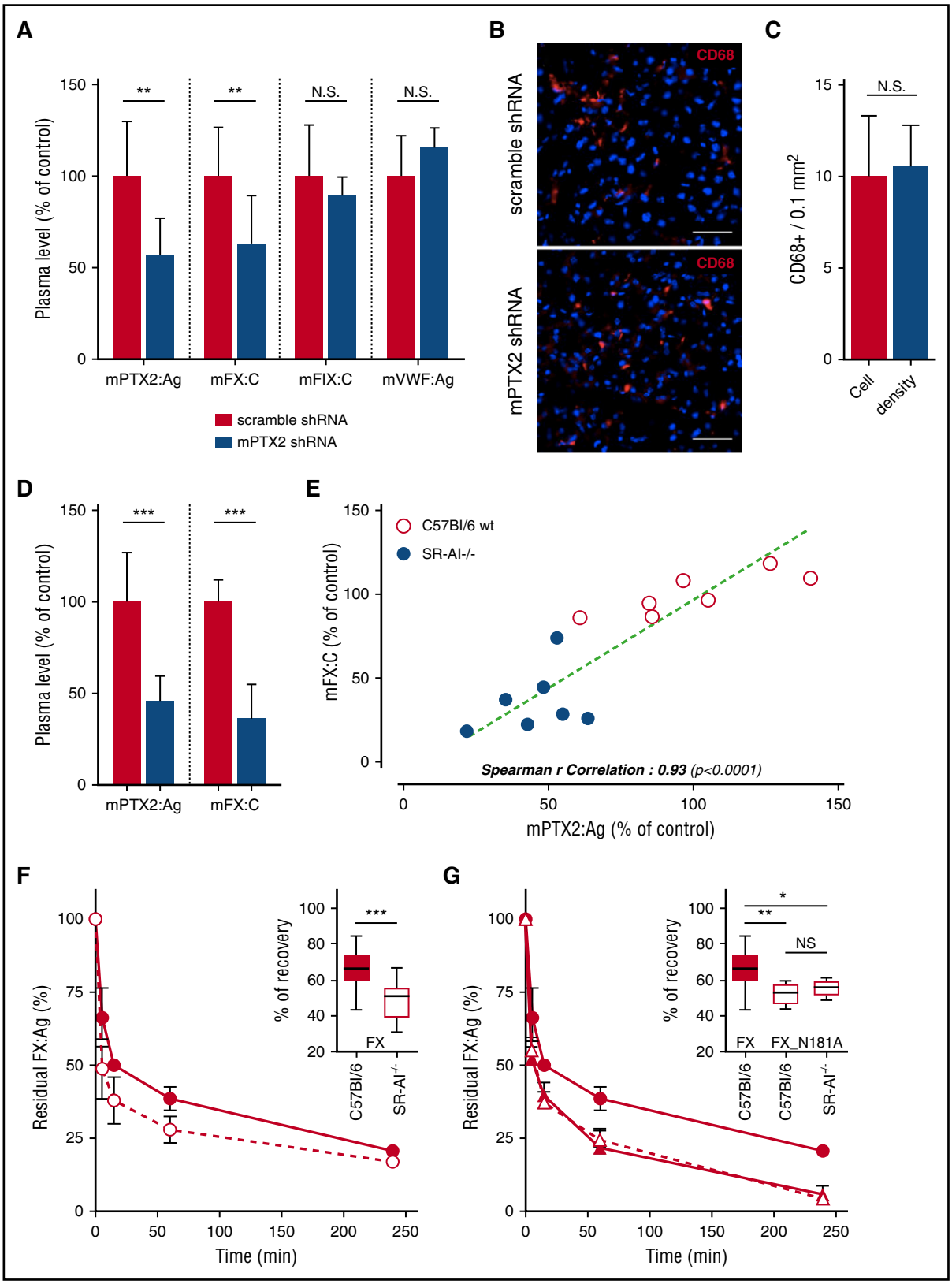

Figure 5. Effect of PTX2 and SR-AI on FX levels and clearance. Hydrodynamic gene delivery of anti-murine PTX2 shRNA in C57Bl/6 mice. Blood was taken by retro-orbital puncture 24 and 48 hours postinjection, and PTX2 antigen, FX and FIX activities, and VWF antigen were measured in the plasma (A). Control was performed using a scramble shRNA construct (red bars). Tissue cryosections of the liver were performed and immunostained for CD68 (B), and macrophages density was subsequently measured (C). Results are presented as the mean ± SD of 5 to 11 mice per condition in 3 different experiments. Representative images were acquired in widefield microscopy (B), objective 40×; bars represent 20 μm. (D) PTX2 antigen levels in plasma of SR-AI–deficient vs wt mice. Results are expressed in a whisker plot where boxes represent the median and 25th to 75th percentile, and bars represent the minimum and maximum of 7 mice per condition. (E) Correlation of PTX2 antigen level and FX activity in the plasma of wt and SR-AI–deficient mice. Spearman's rank correlation coefficient was calculated to assess the statistical dependence of the 2 values. Dots represent each individual

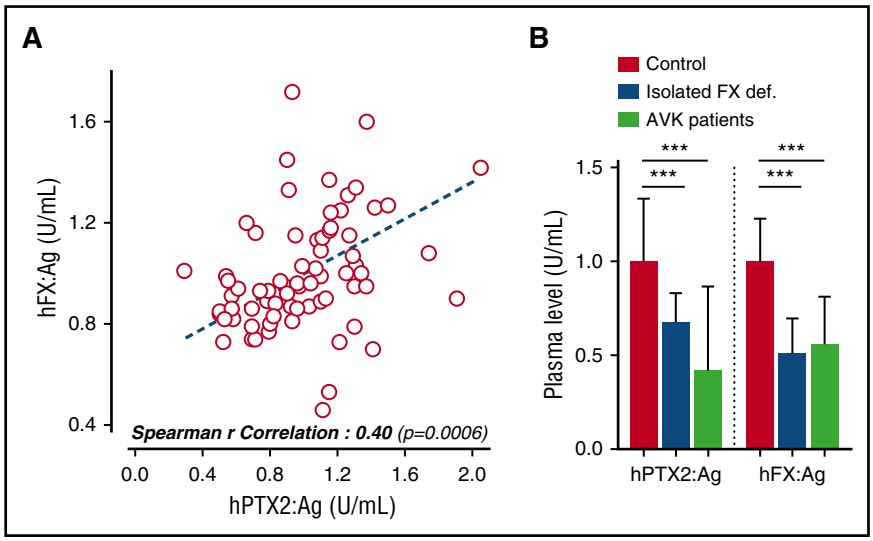

Figure 6. Levels of circulating FX and PTX2 are interdependent in human plasma. (A) PTX2 and FX antigen levels were measured in human plasma samples obtained from random donors (n = 71). Spearman's rank correlation coefficient was calculated to assess the statistical dependence of the 2 values. Dots represent each individual sample. (B) PTX2 and FX antigen levels in patients diagnosed with isolated FX deficiency (blue columns; n = 18) or patients under anti–vitamin K treatment (green columns; n = 35) were compared with random donors. Results are expressed as mean ± SD of 18 to 71 samples per group. ***$P < .001$, statistical significance in a Mann-Whitney nonparametric unpaired test.

The potential of PTX2 to modulate internalization of the FX/SR-AI complex was addressed in reconstitution experiments using SR-AI–transfected HEK293 cells. Only when PTX2 was added to FX was the ternary PTX2/FX/SR-AI complex able to remain at the cell surface, similarly to what was observed upon incubation of FX with THP1-derived macrophages, which contain endogenously expressed PTX2 (Figures 1-3). When assessing FX uptake by SR-AI–transfected HEK293 cells with or without PTX2, no complete overlap in staining for FX and SR-AI or FX and PTX2 was observed (Figure 3A,C). Because FX does not bind to nontransfected HEK293 cells,[14] it is unlikely that incomplete overlap in staining originates from FX binding to unidentified binding sites. Incomplete overlap may be explained by variation in the efficiency by which different proteins are stained in the immunofluorescence procedure. Also, FX may be separated from SR-AI following internalization and targeting to lysosomes, while SR-AI is recycled back to the cell surface. As for PTX2, incomplete complex formation between FX and PTX2 may result in the separate uptake of the individual proteins, in which they end up in separate lysosome vesicles.

We considered that PTX2 may simply block FX binding to SR-AI. However, binding assays showed that a tertiary complex can be formed (Figure 4). Furthermore, when SR-AI–expressing cells were incubated with PTX2 alone, this led to a gradual uptake of PTX2 (Figure 3). Apparently, the formation of the ternary complex is needed to avoid uptake of both PTX2 and FX. The mechanism that keeps the ternary complex at the cell surface waits further elucidation.

A critical step in understanding how PTX2 could modulate the formation of the FX/SR-AI complex is to decipher whether these 3 proteins are able to physically interact. Distinct experimental approaches (direct binding studies and cellular interaction experiments) all point to the possibility that each partner has the potential to interact with both other components of the ternary complex. By using purified proteins, a dose-dependent association was detected for each combination, allowing the calculation of the respective apparent binding constants ($K_{D,app}$) (Figure 4). All binding constants were in the same order of magnitude, ranging from 0.21 to 0.73 μM. Furthermore, the affinity of FX was similar for SR-AI and PTX2 individually compared with the PTX2/SR-AI complex (supplemental Figure 4B-C). Interestingly, binding required the presence of the FX activation peptide including the glycan structure at position N181 (Figure 4F). A consequence is that, once activated, FXa is no longer bound to PTX2, indicating that PTX2 is unlikely to influence FXa function. The involvement of the activation peptide may explain the absence of PTX2 binding by other vitamin K–dependent proteases, like FVII, protein C, and FIX (supplemental Figure 4A), as the activation peptide is poorly conserved between these proteins. It should be noted that PTX2 could potentially affect FX activation. However, we could not observe any difference in FX activation by the tenase and FVIIa/TF complex or by RVV-X protease (Figure 4G). This is in agreement with older studies showing efficient FX activation at the macrophage surface by the FVIIa/TF and the tenase complex.[22]

An intriguing consequence of the calculated binding affinity for PTX2-FX is that based on their respective plasma concentrations, one would expect that at least a portion of both proteins circulates as a macromolecular complex. Indeed, this hypothesis was readily validated in immunoprecipitation experiments using normal human plasma and FX-deficient plasma (Figure 4E-F). To get an indication of the extent of complex formation, immunodepletion experiments were performed using anti-PTX2 antibodies. Using this approach, we could estimate that 53 ± 6% (n = 3) of FX was bound to PTX2 in normal plasma. Assuming molar concentrations of pentameric PTX2 and FX being 0.20 to 0.26 μM and 0.14 to 0.17 μM, respectively, this indicates a stoichiometry of 0.29 to 0.45 mol FX/mol PTX2 pentamer. Irrespective of how much FX is actually associated to PTX2 in the circulation, our findings strongly suggest that plasma levels of PTX2 and FX are interdependent. Via hepatic expression of shRNA targeting PTX2, we were able to reduce PTX2 levels by ~45%. Simultaneously, FX levels were reduced by 37%, while leaving FIX levels unaffected (Figure 5A). It would be of interest to test whether FX levels are similarly decreased

Figure 5 (continued) mice, and bars represent the mean ± SD. (F-G) C57Bl/6 (closed symbols) and SR-AI–deficient mice (open symbols) were injected in the caudal vein with 10 μg of FX (circles) or FX_N181A (triangles). Plasma was collected at different time point (5 minutes, 15 minutes, 1 hour, 4 hours, and 24 hours), and residual FX antigen was measured. Data are presented as percentage antigen relative to the amount injected (mean ± SD; 5 to 10 mice per group). Recoveries are presented separately in a whisker plot where boxes represent the median and 25th to 75th percentile, and bars represent the minimum and maximum (insert in G and F). *$P < .05$, **$P < 0.01$, and ***$P < 0.001$, statistical difference in a Mann-Whitney nonparametric unpaired statistical test.

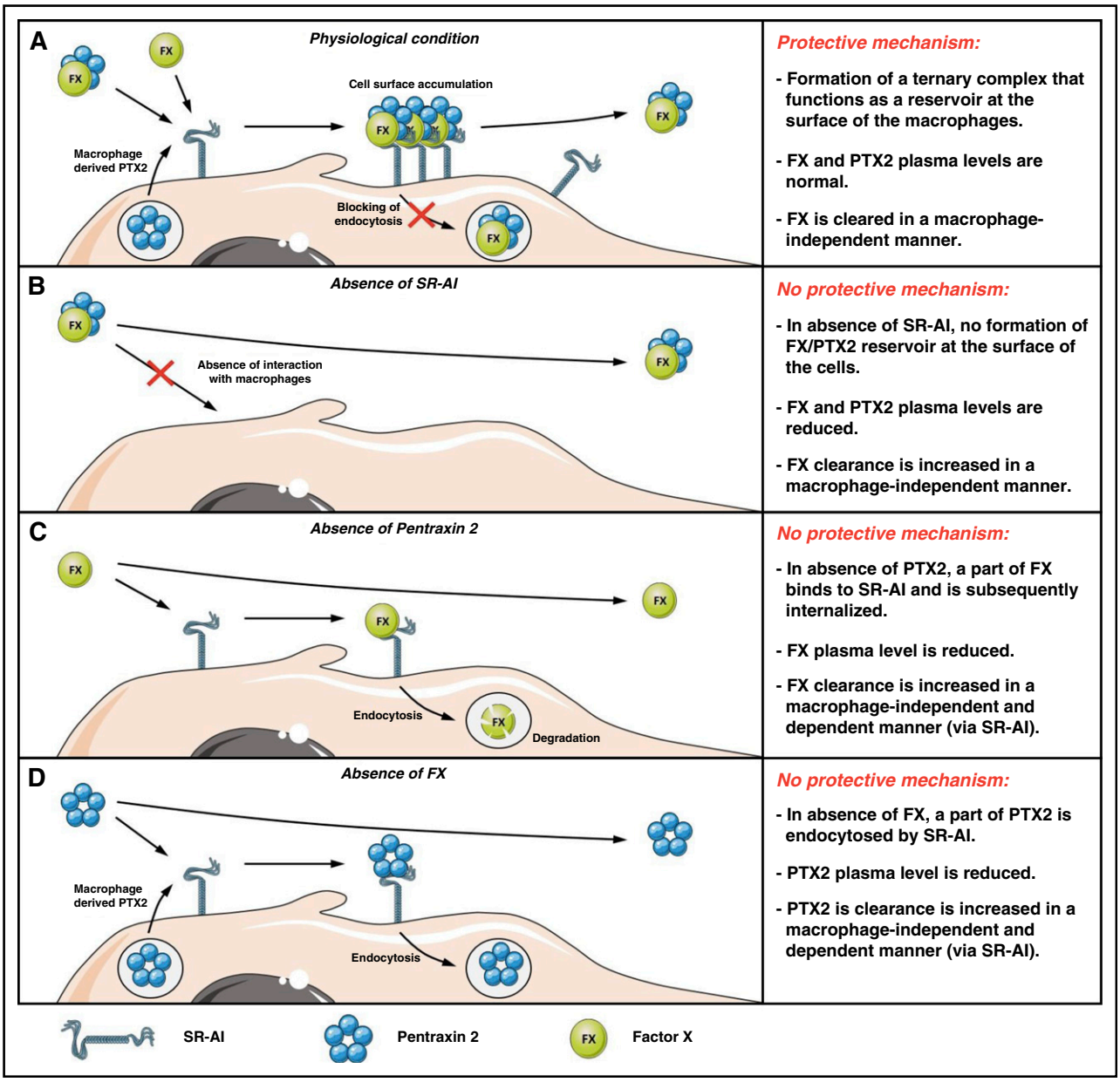

Figure 7. Schematic model of FX regulation by SR-AI and PTX2. (A) Under physiological conditions, part of FX circulates in association with PTX2 as a macromolecular complex. Upon binding to SR-AI at the surface of macrophages, the presence of PTX2 prevents receptor-mediated endocytosis, which results in the protective mechanism that maintains elevated plasma levels of FX. FX that arrives alone at the macrophage surface forms a complex with macrophage-produced PTX2. (B) In the absence of SR-AI, the protective interaction with the macrophages is abolished, which ultimately leads to increased clearance of FX, associated with reduced circulating levels of both FX and PTX2. (C) In the absence of PTX2, FX is no longer protected against SR-AI–mediated endocytosis. Again, the absence of the protective interaction is associated with increased FX clearance (its regular clearance pathway and also in an SR-AI–mediated fashion by macrophages), resulting in reduced plasma concentrations. (D) In the absence of FX, PTX2 is no longer protected against SR-AI–mediated endocytosis. Again, the absence of the protective interaction is probably with increased PTX2 clearance (via its regular clearance pathway and also in an SR-AI–mediated fashion by macrophages), resulting in reduced plasma concentrations.

in PTX2-deficient mice.[23] Interestingly, deficiency of SR-AI was associated with a concurrent reduction of PTX2 and FX, and strong correlation between plasma levels of PTX2 and FX in mice was observed (Figure 5D-E). The correlation between FX and PTX2 plasma levels was also observed in human plasma samples. Analysis of 71 samples from healthy individuals revealed a significant correlation between PTX2 and FX plasma levels (Figure 6A). Moreover, in plasma samples where FX levels were reduced, a concomitant reduction in PTX2 levels were detected as well (Figure 6B).

The interdependency of FX and PTX2 plasma levels was unexpected but may be clinically relevant. Recently, the results of a phase 1 clinical trial using a combination of a small-molecule inhibitor and a humanized anti-PTX2 antibody in the treatment of systemic amyloidosis were reported, demonstrating a >90% reduction in circulating levels of PTX2.[24] It cannot be excluded that in these patients also FX levels have concurrently been reduced, thereby increasing the risk of potential bleeding complications. In the study, no such complications were noted, perhaps because spontaneous bleedings are usually observed only when FX levels arrive below 10%.[25,26] Nevertheless, care should be taken by analyzing FX levels upon PTX2-depleting therapy. Further, some forms of systemic amyloidosis are associated with an acquired FX deficiency.[27] Importantly, FX levels are

reduced to below 0.2 to 0.5 U/mL in a relatively small portion of patients with systemic amyloidosis (5% to 10%).[28,29] This low number is compatible with the observation that PTX2 levels themselves are rarely reduced in these patients.[30-32] The acquired FX deficiency in these patients is probably related to its cotargeting with PTX2 to amyloid plaques, rather than through excessive clearance.

Taken together, we have identified PTX2 as a novel partner for FX, and complex formation is essential to maintain normal plasma levels of FX and to prevent uptake of FX by the macrophage-receptor SR-AI (Figure 7). When SR-AI is absent, no reservoir for FX and PTX2 can be formed at the macrophage surface, and both proteins will be cleared more rapidly in a macrophage-independent manner (Figure 7B). Importantly, by which cells and which receptors FX and PTX2 are removed from the circulation is currently unclear, and additional studies are underway to elucidate these pathways.

We believe that the protective mechanism identified in this study (formation of the ternary FX/PTX2/SR-AI complex that remains at the cell surface) resembles to some extent the protective mechanism for albumin and immunoglobulin G: these proteins are recycled via the FcRn receptor, which allows their long circulatory survival. In FcRn knockout mice, this recycling mechanism no longer exists, and clearance of immunoglobulin G and albumin is accelerated resulting in reduced plasma levels. The difference between both systems is, however, that when the levels of one of the noncellular partners (FX or PTX2) are reduced, insufficient ternary complex is being formed, allowing SR-AI to endocytose PTX2 or FX, which contributes to the increased clearance of these proteins (Figure 7C-D).

Acknowledgments

The authors thank Pascal Roux and Audrey Salles (Imagopole, Institut Pasteur, Paris, France) for their help in acquisition and interpretation of optical microscopy data; Thibault Leger and Camille Garcia (Institut Jacques Monod, Paris, France) for performing mass spectrometry experiments; and Florence Fragnet and Anne-Lisse Marville for their skillful administrative assistance.

This work was supported by an unrestricted research grant from NovoNordisk S/A. They had no role in the design of the study or in the analysis and interpretation of the data.

Authorship

Contribution: V.M., G.A., P.L., A.B., A.H., and C.L. performed experiments; V.M., C.V.D., P.J.L., and O.D.C. designed the study and analyzed data; V.R., M.V., and D.B. provided valuable reagents; V.M., P.J.L., and O.D.C. wrote the manuscript; and all authors contributed to the editing of the final manuscript.

Conflict-of-interest disclosure: P.J.L. provides consultancy to NovoNordisk S/A. The remaining authors declare no competing financial interests.

Correspondence: Peter J. Lenting, INSERM U1176, 80 rue du General Leclerc, 94276 Le Kremlin-Bicêtre, France; e-mail: peter.lenting@inserm.fr.

References

1. Peyvandi F, Mannucci PM. Rare coagulation disorders. *Thromb Haemost*. 1999;82(4):1207-1214.
2. Uprichard J, Perry DJ. Factor X deficiency. *Blood Rev*. 2002;16(2):97-110.
3. Dewerchin M, Liang Z, Moons L, et al. Blood coagulation factor X deficiency causes partial embryonic lethality and fatal neonatal bleeding in mice. *Thromb Haemost*. 2000;83(2):185-190.
4. Lange S, Gonzalez I, Pinto MP, et al. Independent anti-angiogenic capacities of coagulation factors X and Xa. *J Cell Physiol*. 2014;229(11):1673-1680.
5. Livingston JR, Sutherland MR, Friedman HM, Pryzdial EL. Herpes simplex virus type 1-encoded glycoprotein C contributes to direct coagulation factor X-virus binding. *Biochem J*. 2006;393(2):529-535.
6. Doronin K, Flatt JW, Di Paolo NC, et al. Coagulation factor X activates innate immunity to human species C adenovirus. *Science*. 2012;338(6108):795-798.
7. Antoniak S, Mackman N. Multiple roles of the coagulation protease cascade during virus infection. *Blood*. 2014;123(17):2605-2613.
8. Xu Z, Qiu Q, Tian J, et al. Coagulation factor X shields adenovirus type 5 from attack by natural antibodies and complement. *Nat Med*. 2013;19(4):452-457.
9. Waddington SN, McVey JH, Bhella D, et al. Adenovirus serotype 5 hexon mediates liver gene transfer. *Cell*. 2008;132(3):397-409.
10. Borensztajn K, Stiekema J, Nijmeijer S, Reitsma PH, Peppelenbosch MP, Spek CA. Factor Xa stimulates proinflammatory and profibrotic responses in fibroblasts via protease-activated receptor-2 activation. *Am J Pathol*. 2008;172(2):309-320.
11. Krupiczojc MA, Scotton CJ, Chambers RC. Coagulation signalling following tissue injury: focus on the role of factor Xa. *Int J Biochem Cell Biol*. 2008;40(6-7):1228-1237.
12. Scotton CJ, Krupiczojc MA, Königshoff M, et al. Increased local expression of coagulation factor X contributes to the fibrotic response in human and murine lung injury. *J Clin Invest*. 2009;119(9):2550-2563.
13. Kurdi M, Cherel G, Lenting PJ, Denis CV, Christophe OD. Coagulation factor X interaction with macrophages through its N-glycans protects it from a rapid clearance. *PLoS One*. 2012;7(9):e45111.
14. Muczynski V, Bazaa A, Loubière C, et al. Macrophage receptor SR-AI is crucial to maintain normal plasma levels of coagulation factor X. *Blood*. 2016;127(6):778-786.
15. van Schooten CJ, Shahbazi S, Groot E, et al. Macrophages contribute to the cellular uptake of von Willebrand factor and factor VIII in vivo. *Blood*. 2008;112(5):1704-1712.
16. Fortin A, Penman M, Stevenson MM, Krieger M, Gros P. Identification and characterization of naturally occurring variants of the macrophage scavenger receptor (SR-A). *Mamm Genome*. 2000;11(9):779-785.
17. Kelley JL, Ozment TR, Li C, Schweitzer JB, Williams DL. Scavenger receptor-A (CD204): a two-edged sword in health and disease. *Crit Rev Immunol*. 2014;34(3):241-261.
18. Marx I, Lenting PJ, Adler T, Pendu R, Christophe OD, Denis CV. Correction of bleeding symptoms in von Willebrand factor-deficient mice by liver-expressed von Willebrand factor mutants. *Arterioscler Thromb Vasc Biol*. 2008;28(3):419-424.
19. Baltz ML, Gomer K, Davies AJ, Evans DJ, Klaus GG, Pepys MB. Differences in the acute phase responses of serum amyloid P-component (SAP) and C3 to injections of casein or bovine serum albumin in amyloid-susceptible and -resistant mouse strains. *Clin Exp Immunol*. 1980;39(2):355-360.
20. Tatsuta E, Sipe JD, Shirahama T, Skinner M, Cohen AS. Different regulatory mechanisms for serum amyloid A and serum amyloid P synthesis by cultured mouse hepatocytes. *J Biol Chem*. 1983;258(9):5414-5418.
21. Klein I, Cornejo JC, Polakos NK, et al. Kupffer cell heterogeneity: functional properties of bone marrow derived and sessile hepatic macrophages. *Blood*. 2007;110(12):4077-4085.
22. McGee MP, Li LC. Functional difference between intrinsic and extrinsic coagulation pathways. Kinetics of factor X activation on human monocytes and alveolar macrophages. *J Biol Chem*. 1991;266(13):8079-8085.
23. Botto M, Hawkins PN, Bickerstaff MC, et al. Amyloid deposition is delayed in mice with targeted deletion of the serum amyloid P component gene. *Nat Med*. 1997;3(8):855-859.
24. Richards DB, Cookson LM, Berges AC, et al. Therapeutic clearance of amyloid by antibodies to serum amyloid P component. *N Engl J Med*. 2015;373(12):1106-1114.
25. Brown DL, Kouides PA. Diagnosis and treatment of inherited factor X deficiency. *Haemophilia*. 2008;14(6):1176-1182.
26. Girolami A, Cosi E, Santarossa C, Ferrari S, Girolami B, Lombardi AM. Prevalence of bleeding manifestations in 128 heterozygotes for Factor X deficiency, mainly for FX Friuli,

matched versus 128 unaffected family members, during a long sequential observation period (23.5 years). *Eur J Haematol*. 2016; 97(6):547-553.

27. Furie B, Greene E, Furie BC. Syndrome of acquired factor X deficiency and systemic amyloidosis in vivo studies of the metabolic fate of factor X. *N Engl J Med*. 1977;297(2): 81-85.
28. Mumford AD, O'Donnell J, Gillmore JD, Manning RA, Hawkins PN, Laffan M. Bleeding symptoms and coagulation abnormalities in 337 patients with AL-amyloidosis. *Br J Haematol*. 2000;110(2): 454-460.
29. Choufani EB, Sanchorawala V, Ernst T, et al. Acquired factor X deficiency in patients with amyloid light-chain amyloidosis: incidence, bleeding manifestations, and response to high-dose chemotherapy. *Blood*. 2001;97(6): 1885-1887.
30. Skinner M, Vaitukaitis JL, Cohen AS, Benson MD. Serum amyloid P-component levels in amyloidosis, connective tissue diseases, infection, and malignancy as compared to normal serum. *J Lab Clin Med*. 1979;94(4): 633-638.
31. Gertz MA, Skinner M, Cohen AS, Kyle RA. Nephelometric measurement of human serum amyloid P component (SAP). *J Lab Clin Med*. 1983;102(5):773-778.
32. Hawkins PN, Tennent GA, Woo P, Pepys MB. Studies in vivo and in vitro of serum amyloid P component in normals and in a patient with AA amyloidosis. *Clin Exp Immunol*. 1991;84(2): 308-316.